Three-dimensional displacement-length scaling and maximum dimension of normal faults in layered rocks

Roger Soliva,[1,2] Richard A. Schultz,[1] and Antonio Benedicto[3]

[1] We analyze the magnitudes and distributions of displacements on normal faults that are contained within a five layer marly-limestone/silty-clay sedimentary sequence. Observations of bedding plane exposures of the well-exposed mechanically isolated faults reveal a systematic strong decrease in the displacement gradient related to the horizontal lengthening of faults growing at constant height. Because mechanically heterogeneous sequences produce populations of vertically restricted faults having a large range of aspect ratios (length/downdip height), much of the scatter on a displacement-length diagram can be attributed to nonlinear growth paths. Our results demonstrate the significant influence of layering on fault scaling relations, growth, and maximum dimensions. **Citation:** Soliva, R., R. A. Schultz, and A. Benedicto (2005), Three-dimensional displacement-length scaling and maximum dimension of normal faults in layered rocks, *Geophys. Res. Lett.*, *32*, L16302, doi:10.1029/2005GL023007.

1. Introduction

[2] Fracture populations commonly show strongly variable displacement-length ratios mainly because of (1) long- and short-range mechanical interactions [e.g., *Olson*, 1993; *Gupta and Scholz*, 2000], (2) linkage [e.g., *Cartwright et al.*, 1995] or (3) variations in rock properties [*Bürgmann et al.*, 1994; *Bai and Pollard*, 2000]. The role of rock layering on 3-D scaling and dimensions of joints [e.g., *Olson*, 2003], deformation bands [*Schultz and Fossen*, 2002], and earthquake ruptures [*Wilkins and Schultz*, 2005] has been demonstrated, and its importance on the growth of faults is now becoming increasing recognized.

[3] Recent observations of faults in layered rock sequences show that both rigid or plastic layers can provide barriers to fault propagation [*Wilkins and Gross*, 2002; *Soliva and Benedicto*, 2005], suggesting that normal fault vertical restriction can occur at different levels of a sedimentary sequence. If multiple levels of restriction occur [*Benedicto et al.*, 2003], then 3-D fault propagation, termination and therefore characteristic maximum displacement – length (D_{max}-L) scaling measured on horizontal planes should be influenced by the stratification. In this paper (1) we demonstrate consistency between D_{max}-L data and 3-D scaling relations, (2) we illustrate the control of stratification on displacement gradient variations, and (3) we discuss how horizontal propagation and maximum length depend on fault growth with constant downdip height (H).

2. Studied Faults

[4] The normal faults are observed on a $30-70°$ dipping bedding plane of early Maestrichtian continental limestone in the lignite quarry from the "Collado de Fumanyá" (Catalonia, Spain). More than 500 fault scarps of metric to decametric trace length, with an average dip angle relative to bedding of $60°$, are observed within a 4.5 m thick carbonate sequence composed of two marly-limestone units of thicknesses $T_1 \sim 2$ m, which are bounded and interbedded by silty-clay layers. Observations from different cross-sectional exposures reveal that many faults terminate within overlying and underlying meter scale thick silty-clay layers and also in the intermediate 45 cm thick clay rich level (Figure 1). On the bedding surface, the faults are evenly spaced ($2-3$ m) and show a negative exponential size distribution with maximum observed length of 42.6 m [*Soliva and Benedicto*, 2005]. *Soliva and Benedicto* [2005] and *Soliva et al.* [2005] provide detailed description of fault scarp morphology, photographs of faults terminations in different layers, and a discussion of the Pyrenean tectonic setting.

[5] We focus our analysis of displacement on isolated half faults observed on the same bedding plane. Isolated half faults are defined as fault surfaces of half length a, the distance measured between D_{max} and fault tip, showing no evidence of interaction with other surrounding faults, i.e. without a displacement gradient increase due to relay ramp, branching, or other evidence for displacement transfer. These faults are always spaced by a minimum distance of two meters to any surrounding fault, the common distance of freely overlapping faults between which relay ramps are never observed. Displacements along fault scarps were measured on photomosaics and were calibrated by both tape and laser theodolite measurements. The small amount of erosion gives an error in displacement that does not exceed ±1 cm.

3. 3-D Scaling of the Fault Population

[6] *Soliva and Benedicto* [2005] show that linear D_{max}-L trends and linear displacement profiles (i.e. faults of $D_{max} <$ 20 cm, Figures 2a and 2b, green) both indicate that the faults grew freeley within a layer (here T_1). In contrast, larger faults exhibiting a shallower trend (blue and red symbols) and flat topped profiles [e.g., *Dawers et al.*, 1993] are vertically restricted by clay layers (Figures 1, 2a

[1]Department of Geological Sciences and Engineering, University of Nevada, Reno, Nevada, USA.
[2]Now at Université Montpellier II, Département des Sciences de la Terre et de l'Environnement, Montpellier, France.
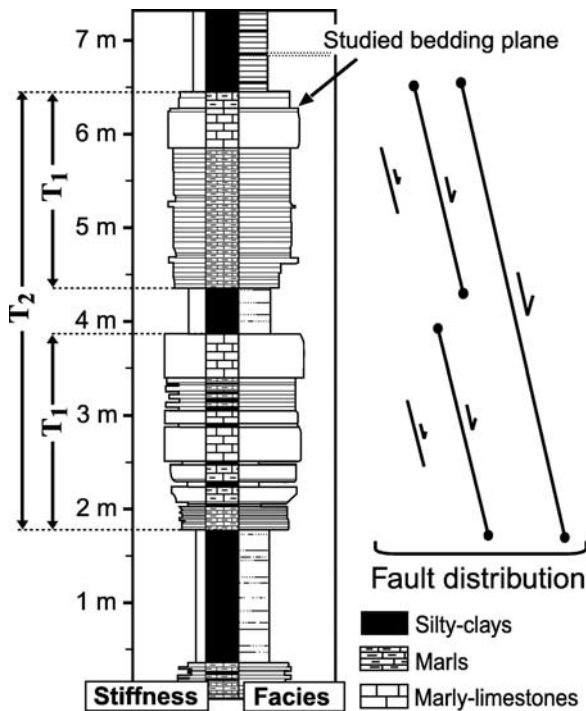[3]Département des Sciences de la Terre, Université Paris-Sud, Orsay, France.

Figure 1. Schematic distribution of faults observed in cross sections of the stratigraphic sequence. Nonrestricted faults are distinguished from faults terminating at the limits of brittle marly-limestone units of thicknesses T_1 and T_2.

and 2b). Additional measurements of faults clarify the data scatter previously observed [*Soliva and Benedicto*, 2005, Figure 3]. The blue and the red datasets distinguish faults restricted at the limits of T_1 from those restricted at the limits of T_2, which have greater displacement. The mean value of D_{max} within the red fault set is about twice the value of the blue one (Figure 2b), revealing the dependence of displacement on the down-dip fault height (H).

[7] In order to quantitatively investigate the influence of proportional (constant L/H) and non-proportional (variable L/H) growth on D_{max}-L scaling, we use the scaling law between D_{max} and fault dimensions proposed by *Schultz and Fossen* [2002]. This analytical solution assumes a shear strength decrease from the tip toward the fault center [e.g., *Cowie and Scholz*, 1992; *Bürgmann et al.*, 1994] and depends on the properties of the surrounding rock (yield strength σ_y, shear modulus G and Poisson's ratio v, the driving stress (σ_d) and a and b the fault semi-axes (i.e. $L = 2a$ and $H = 2b$). To estimate the rock properties at the time of the fault growth, we choose $G = 750$ MPa and $v = 0.32$, which are values for calcareous shales [*Hatheway and Kiersch*, 1989]. The yield strength can be estimated using the stress state of faulting at a depth of ~ 800 m [*Soliva et al.*, 2005], giving $\sigma_y \sim 50$ MPa using laboratory testing of similar carbonate rocks [*Renner and Rummel*, 1996].

[8] The material parameters cited above and a value of $\sigma_d = 28$ MPa ($\sigma_y/\sigma_d \sim 2$, consistent with weak rocks as marly-limestones [*Schultz and Fossen*, 2002]) produce an acceptable fit to the displacement-length data as shown in Figure 2a. A straight line of proportional growth with $L/H = 2$, the aspect ratio expected for nonrestricted faults

[*Soliva and Benedicto*, 2005] and a common value for faults in sedimentary sequences [e.g., *Nicol et al.*, 1996], is consistent with the smallest faults (green dataset). For larger lengths (blue and red) a single non proportional growth curve (constant $H = 2b$) does not account for the wide scatter. However, a fit of $H = 5$ m, relevant to observations of fault terminations at the limits of T_2 ($H = T/\sin \beta = 5$ m, with $T = 4.5$ m and fault dip $\beta \sim 60°$), closely fits the faults of largest height (red dots). Another fit with $H = 2$ m, consistent with the faults terminating in the intermediate silty-clay layer, fits the faults of intermediate height (blue dots). Here, both the data and the curves reveal that the short dimension (height) of the fault is of major importance for D_{max}-L scaling and suggest that the effects of rock properties contrasts on the scaling relations are secondary [e.g., *Bai and Pollard*, 2000].

4. 3-D Growth and Maximum Fault Length

[9] Two end-member cases of fault growth are suggested by our results: single and double confinement (Figures 2c and 2d). In the single confinement case, we infer from Figures 2a and 2b that faults develop first by nearly proportional growth (or radial propagation) with an aspect ratio $L/H \sim 2$ (here called Stage 1). The green fault set, which probably includes faults initiated at the top of the sequence and pinned at this overlying barrier [see *Soliva et al.*, 2005], exhibits both linear displacement profiles and D_{max}-L scaling consistent with $L/H \sim 2$. Indeed, flat topped profiles only occur when the fault aspect ratio exceeds 2. When $H \sim 2$ m, the faults reach and crosscut the intermediate transient barrier (thin clay rich layer) and grow in the lower unit by downward propagation and/or by linkage with a fault present just below [e.g., *Koledoye et al.*, 2000] (Stage 2). Since displacement magnitude is very sensitive to the short fault dimension [e.g., *Schultz and Fossen*, 2002], the increase of fault height leads to an increase in the D_{max}/L ratio. Finally, when $H \sim 5$ m, the thick upper and lower clay layers restrict further vertical fault growth; the faults are then confined and grow horizontally by lengthening towards L_{max} (or the maximum half length $a_{max} \sim 25$ m), the value of maximum length observed for isolated faults in the field area (Stage 3).

[10] In the double confinement case, when $H \sim 2$ m, the faults are restricted at the upper and the intermediate barriers. The faults then grow by lengthening towards L'_{max} (or $a'_{max} \sim 11$ m), the maximum length observed for this layer (Stage 2). In most of the cases (red dataset on Figure 2) the persistence of the intermediate level as a barrier has been temporary, then it is probable that some of the faults were able to cut through it (broken lines, Stage 3). Finally, the faults are restricted at the bounding levels of the carbonate series and can only grow by lengthening toward L_{max}. Here, the mechanical barriers in the stratification cause the fault aspect ratio to increase significantly, consistent with the observed profiles (linear vs. flat topped) and the associated reduction in displacement gradient with length (Figures 2a and 2b).

[11] Maximum lengths are demonstrated in the fault population since the bedding exposure exceeds three times a_{max} and six times a'_{max}. The simplest explanation that can
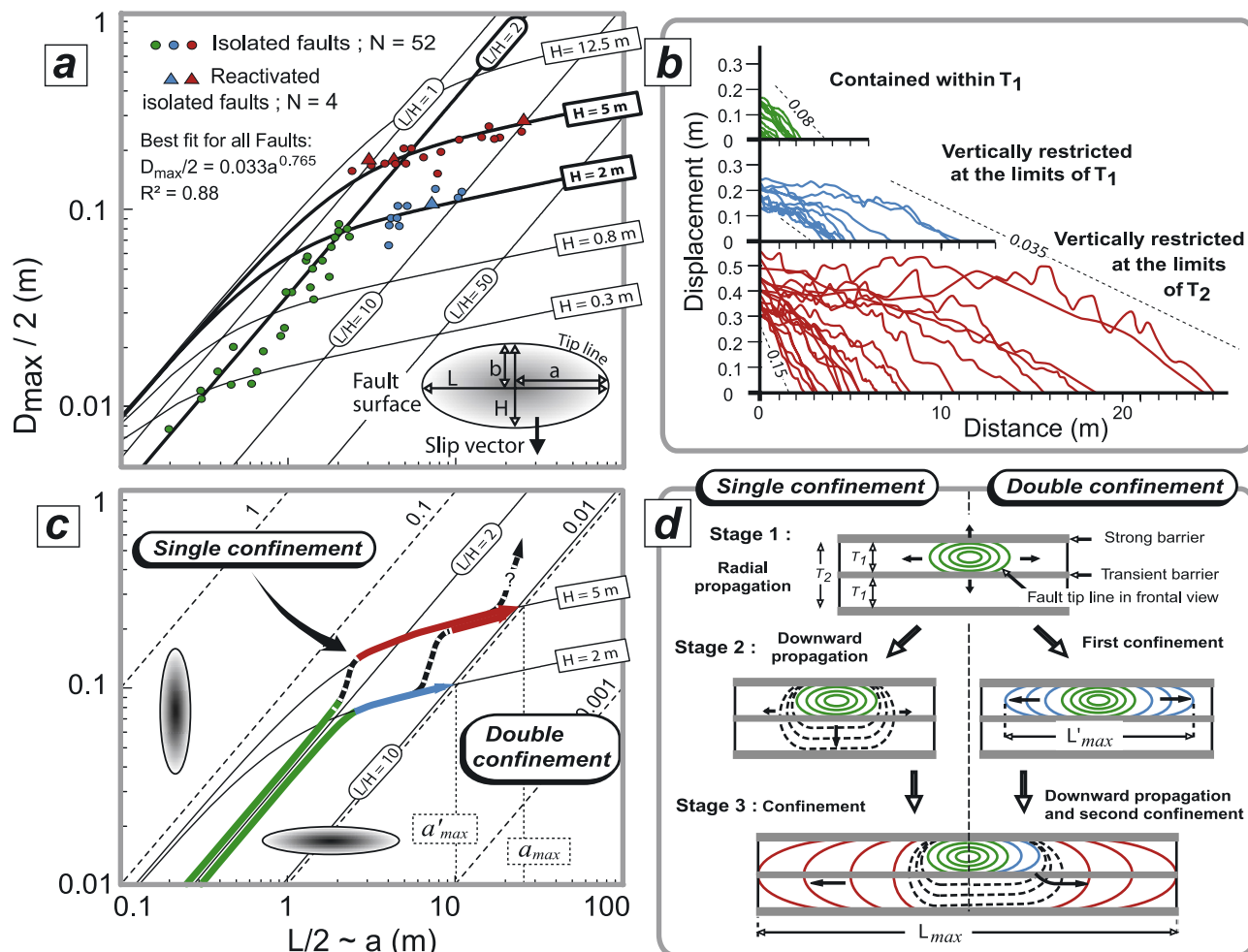
Figure 2. (a) D_{max}-L plot of the studied faults constructed with half-length ($L/2 = a$) and half displacement ($D_{max}/2$). Lines (L/H = constant) and curves (H = constant) are calculated following *Schultz and Fossen* [2002]. (b) Displacement profiles along the bedding for the isolated faults shown in (a). Interpreted (c) D_{max}-L paths and (d) growth sequence. The color code corresponds to the three faults sets distinguished in Figure 1, green: nonrestricted, blue: restricted at the limits of T_1, and red: restricted at the limits of T_2.

be invoked to inhibit further horizontal fault propagation (beyond a maximum length) is a decrease in the remote driving stress. However, this somewhat ad hoc solution does not explain the fact that both observed maximum lengths correspond to the same fault aspect ratio ($L/H \sim 10$) (Figure 2a). Instead, we hypothesize that a critical maximum aspect ratio is responsible for the maximum length, which therefore depends on the layer thickness. What is required to sustain the propagation of an isolated fault is a critical value of near tip displacement gradient leading to an amount of fault tip stress equal to the rock's yield strength [*Cowie and Scholz*, 1992; *Bürgmann et al.*, 1994; *Gupta and Scholz*, 2000]. Therefore, a possible mechanism to inhibit the horizontal propagation and that satisfies field observations is a reduction in the horizontal displacement gradient below some threshold value in association with the demonstrated increase of fault aspect ratio. Figure 3 shows a positive correlation between fault end gradient and D_{max}/L data of the restricted faults, which implies that both of these parameters decreased together during fault lengthen-

ing. The faults close to their maximum lengths (i.e. on the line of $L/H = 10$, Figure 2a) show similar and relatively low values of D_{max}/L (~ 0.01) and fault end gradient <0.05 (Figure 3). Although the physical mechanisms for the decrease of fault end gradient remain to be explored, the evidence for end gradient decrease with lengthening of a vertically restricted fault is unambiguously demonstrated by the fault displacement profiles. These faults reveal a substantial decrease in end gradient during lengthening (from 0.235 to 0.03) suggesting that fault propagation was not possible below a minimum end gradient ~ 0.03, corresponding to $D_{max}/L \sim 0.01$ or $L/H \sim 10$.

5. Conclusions

[12] Although scatter in D_{max}-L data for a particular fault population is commonly attributed to fault interaction and linkage, the Fumanyá fault population shows variation in D_{max}/L and fault end displacement gradient close to one order of magnitude (about three times the variation due to
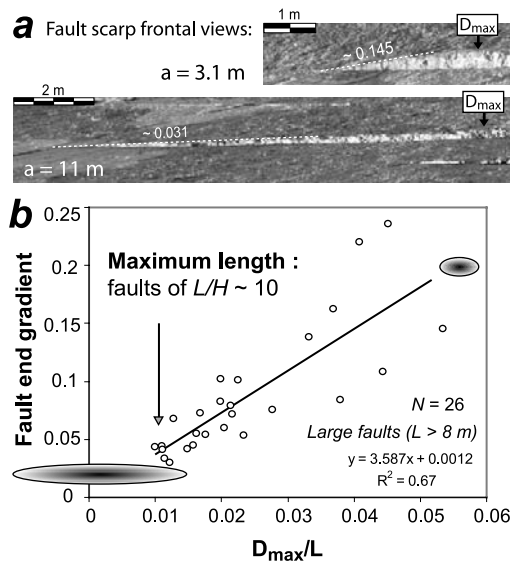
Figure 3. (a) Examples of end displacement gradients on isolated fault scarps for nonrestricted (a = 3.1 m, gradient = 0.145) and vertically restricted faults (a = 11 m, gradient = 0.031). (b) End gradient vs. D_{max}/L plot of the vertically restricted faults from Figure 2b. Fault ends are the linear parts between deflection zone and fault tip of the flat topped displacement profiles.

fault interaction and linkage in the same fault population [*Soliva and Benedicto*, 2004, Figure 8]) that is not related to measurement errors or to fault interaction and linkage. Both field observations and new modelling reveal that these variations are intimately related to the short dimension (height) of faults restricted by silty-clay layers, whose ability to propagate horizontally diminishes with fault lengthening.

[13] Because (1) strong rheological contrasts and (2) large fault aspect ratios (up to 11) can be commonly inferred in sedimentary sequences [e.g., *Cartwright et al.*, 1995] and at the crustal scale [e.g., *Cowie et al.*, 1994; *dePolo*, 1998], we suggest that similar behavior, and the associated 3-D scaling relations, should apply in various settings and for larger fault systems. Transient vertical restriction of faults within a heterogeneous rheological alternation therefore constitutes a possible explanation for why some fault systems exhibit very large scatter in D_{max}-L [e.g., *Schlische et al.*, 1996], especially where the scaling exponent is less than 1, and where faults are flat topped and have low-end gradients [e.g., *Cowie et al.*, 1994; *Manighetti et al.*, 2001; *Schultz and Fossen*, 2002]. We expect that fracture populations of any type (e.g., earthquake ruptures, faults, joints, deformation bands) will exhibit similar characteristics when vertical growth and accumulation of displacement are hindered by rheological layering.

References

Bai, T., and D. D. Pollard (2000), Fracture spacing in layered rocks: A new explanation based on the stress transition, *J. Struct. Geol.*, *22*, 43–57.

Benedicto, A., R. A. Schultz, and R. Soliva (2003), Layer thickness and the shape of faults, *Geophys. Res. Lett.*, *30*(20), 2076, doi:10.1029/2003GL018237.

Bürgmann, R., D. D. Pollard, and S. J. Martel (1994), Slip distributions on faults: Effects of stress gradients, inelastic deformation, heterogeneous host-rock stiffness, and fault interaction, *J. Struct. Geol.*, *16*, 1675–1690.

Cartwright, J. A., B. Trudgill, and C. S. Mansfield (1995), Fault growth by segment linkage: An explanation for scatter in maximum displacement and trace length data from the Canyonlands Grabens of SE Utah, *J. Struct. Geol.*, *17*, 1319–1326.

Cowie, P. A., and C. H. Scholz (1992), Physical explanation for the displacement-length relationship of fault using a post-yield fracture mechanics model, *J. Struct. Geol.*, *14*, 1133–1148.

Cowie, P. A., A. Malinverno, W. B. F. Ryan, and M. H. Edwards (1994), Quantitative fault studies on the East Pacific Rise: A comparison of sonar imaging techniques, *J. Geophys. Res.*, *99*, 15,205–15,218.

Dawers, N. H., M. H. Anders, and C. H. Scholz (1993), Growth of normal faults: Displacement-length scaling, *Geology*, *21*, 1107–1110.

dePolo, C. M. (1998), A reconnaissance technique for estimating the slip rates of normal-slip faults in the Great Basin, and application to faults in Nevada, USA, Ph.D. thesis, 223 pp., Univ. of Nev., Reno.

Gupta, A., and C. H. Scholz (2000), A model of normal fault interaction based on observation and theory, *J. Struct. Geol.*, *22*, 865–879.

Hatheway, A. W., and G. A. Kiersch (1989), Engineering properties of rock, in *Practical Handbook of Physical Properties of Rocks and Minerals*, edited by R. S. Carmichael, pp. 672–715, CRC Press, Boca Raton, Fla.

Koledoye, A. B., A. Aydin, and E. May (2000), Three dimensional visualization of normal fault segmentation and its implication for fault growth, *Leading Edge*, *19*, 691–701.

Manighetti, I., G. C. P. King, Y. Gaudemer, C. H. Scholz, and C. Doubre (2001), Slip accumulation and lateral propagation of active normal faults in Afar, *J. Geophys. Res.*, *106*, 13,667–13,696.

Nicol, A., J. J. Watterson, J. Walsh, and C. Childs (1996), The shapes, major axis orientations and displacement patterns of fault surfaces, *J. Struct. Geol.*, *18*, 235–248.

Olson, J. E. (1993), Joint pattern development: Effects of subcritical crack growth and mechanical interaction, *J. Geophys. Res.*, *13*, 98, 12,251–12,266.

Olson, J. E. (2003), Sublinear scaling of fracture aperture versus length: An exception or the rule?, *J. Geophys. Res.*, *108*(B9), 2413, doi:10.1029/2001JB000419.

Renner, J., and F. Rummel (1996), The effect of experimental and microstructural parameters on the transition from brittle failure to cataclastic flow of carbonate rocks, *Tectonophysics*, *258*, 151–169.

Schlische, R. W., S. S. Young, R. V. Ackermann, and A. Gupta (1996), Geometry and scaling relations of a population of very small rift-related normal faults, *Geology*, *24*, 683–686.

Schultz, R. A., and H. Fossen (2002), Displacement-length scaling in three dimensions: The importance of aspect ratio and application to deformation bands, *J. Struct. Geol.*, *24*, 1389–1411.

Soliva, R., and A. Benedicto (2004), A linkage criterion for segmented normal faults, *J. Struct. Geol.*, *12*, 2251–2267.

Soliva, R., and A. Benedicto (2005), Geometry, scaling relations and spacing of vertically restricted normal faults, *J. Struct. Geol.*, *27*, 317–325.

Soliva, R., A. Benedicto, P. Vergély, and T. Rives (2005), Mechanical control of a lithological alternation on normal fault morphology, growth and reactivation, *Bull. Soc. Geol. Fr.*, 329–341.

Wilkins, S. J., and M. R. Gross (2002), Normal fault growth in layered rocks at Split Mountain, Utah: Influence of mechanical stratigraphy on dip linkage, fault restriction and fault scaling, *J. Struct. Geol.*, *24*, 1413–1429.

Wilkins, S. J., and R. A. Schultz (2005), 3-D cohesive end zone model for source scaling of strike-slip intraplate earthquakes, *Bull. Seismol. Soc. Am.*, in press.

———————————
A. Benedicto, Dept. des Sciences de la Terre, Université Paris-Sud, UMR 7072, F-91405 Orsay, France. (benedicto@geol.u-psud.fr)

R. A. Schultz, Department of Geological Sciences and Engineering/172, University of Nevada, Reno, NV 89557, USA. (schultz@mines.unr.edu)

R. Soliva, Université Montpellier II, Bat. 22, Place E. Bataillon, F-34095 Montpellier, France. (solivaroger@yahoo.fr)